Chapter 5

Microcontact printing methods for molecular electronics applications

5.1   Introduction

Microcontact printing (µCP) is a highly versatile technique for patterning surfaces using monolayers with submicron resolution.[1] Like other soft lithography techniques, µCP is based on replicating a pattern from a flexible, elastomeric stamp to a surface. In this method, the pattern is transferred by coating the stamp with a molecule capable of forming a covalent bond with the surface and forming an intimate contact between the two materials (Figure
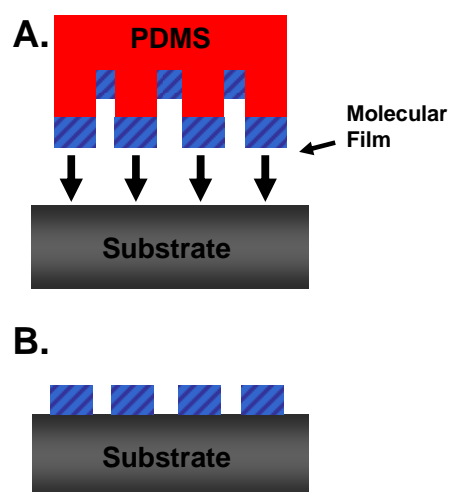
Figure 5.1. Schematic of microcontact printing. **A.** A PDMS stamp coated with an ink solution is brought into contact with a substrate. **B.** The ink covalently attaches to the substrate and the stamp is removed.

5.1A). Due to high local concentration of the molecules, a monolayer rapidly forms on the surface, replicating the pattern on the stamp (Figure 5.1B).

There are several applications for μCP. As an alternative to conventional lithography, μCP has been used to pattern self-assembled monolayers (SAMs) as ultrathin wet etch resists[2, 3] and as templates for the growth or deposition of materials[4]. The flexible nature of the elastomeric stamp also facilitates the patterning on non-planar surfaces, leading to applications in a variety of fields including optics and MEMS.[1]

The key to μCP's success is in its highly simple, high throughput and inexpensive nature. μCP is a bottom-up fabrication technique. Since surface structures are added, not removed, very little waste is generated. Conventional lithography, in contrast, consists of applying a resist and then removing patterns from it. Both the resist and the resist developer are toxic chemicals and generate hazardous waste. Another benefit to μCP is that very large areas can be patterned easily by using a large planar stamp or a rolling stamp (analogous to a paint roller).[1] Standard lithography techniques become progressively more expensive as the exposure area increases. Lastly, the materials involved with μCP: the elastomer stamp (typically polydimethylsiloxane), the ink molecule, and the ink solvent (usually a standard solvent in organic synthesis like acetonitrile) are all inexpensive and quick to assemble. In contrast, the instruments, facilities, and masks used in conventional lithography are very expensive and require specialized training. Thus, μCP is a promising technique for micro- and nanofabrication.

Recently, μCP has been used to facilitate covalent attachments of new molecules to existing SAMs using chemistries such as Cu-catalyzed azide-alkyne cycloaddition, [5, 6] imine bond formation,[7–9] and amide bond formation.[10–12] In this technique, molecules are

stamped on an existing monolayer. The highly confined interface between the stamp and the substrate promotes a reaction between the ink and monolayer, often times with reaction rates much faster than the analogous solution-based reaction and without an added catalyst.[11] This methdology has been used to pattern oligonucleotides for microassays and biosensors,[6, 9] immobilize cells to study cell-cell and cell-surface interactions,[8] generate peptide arrays for proteins studies,[11] and biological ligands for immunoassays and biosensors.[12]

5.1.1 Application for high-density molecular circuits

Covalent surface attachment using μCP has great potential for applications outside of biology as well. In particular, it may be a useful tool in the fabrication of high-density molecular circuits. In 2007, Green et al. described a molecular electronic circuit using a silicon nanowire (Si NW) crossbar array and a monolayer of amphiphilic, bistable [2]rotaxanes as the active memory element.[13] The development of Si NW devices[14] and circuits[15] was described in Chapters 2–4.

The [2]rotaxanes, assembled in molecular switch tunnel junctions (MSTJs), have been shown to switch between a low conductance state and a high conductance state by the mechanical shuttle of
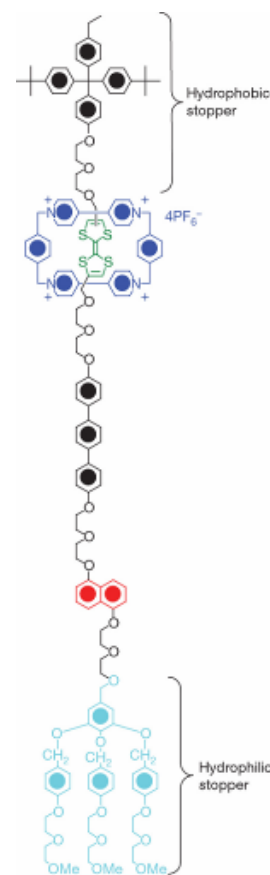
Figure 5.2. Molecular structure of a amphiphilic, bistable [2]rotaxane

the tetracationic cyclophane ring (shown in blue in Figure 5.2) from the tetrathiafulvalene site (shown in green) to the dioxynapthalene site (shown in red).[16, 17] This mechanical shuttle occurs when the tetrathiafulvalene (TTF) group is oxidized by applying a large bias across the solid-state device electrodes. The current levels are then "read" by applying a small, non-perturbing bias.

Although the [2]rotaxane memory devices have been successfully demonstrated, the integration of the monolayer into the device has to be done carefully.[18] The [2]rotaxanes are compressed and aligned via the Langmuir-Blodgett technique and transferred to the bottom electrodes of the memory circuit. The top electrodes are then carefully deposited on top of the monolayer. If the monolayer is compressed at the wrong pressure, the MSTJ fails. Also, the use of the Langmuir-Blodgett technique places design constraints on the molecule and the substrate and the molecules are not covalently attached to the electrodes.

μCP would be a convenient alternative to the Langmuir-Blodgett method for patterning molecular electronic devices directly onto electrode surfaces. This technique has the benefit that the attachment would be covalent, which may lead to better device performance and longer performance times. For instance, this technique may allow the sequential, solvent-free synthesis of [2]rotaxanes directly on devices. Figure 5.3 shows a proposed synthetic sequence. The [2]rotaxane backbone containing the TTF and dioxynapthalene (DNP) sites would be covalently attached to the surface using μCP. The tetracationic cyclophane ring (CBPQT^{4+}) would be stamped next, and the electrostatic interactions between the ring and the rotaxane backbone would promote a threading

process. The stopper (which prevents the ring from slipping off the backbone) would then be stamped and covalently attached.
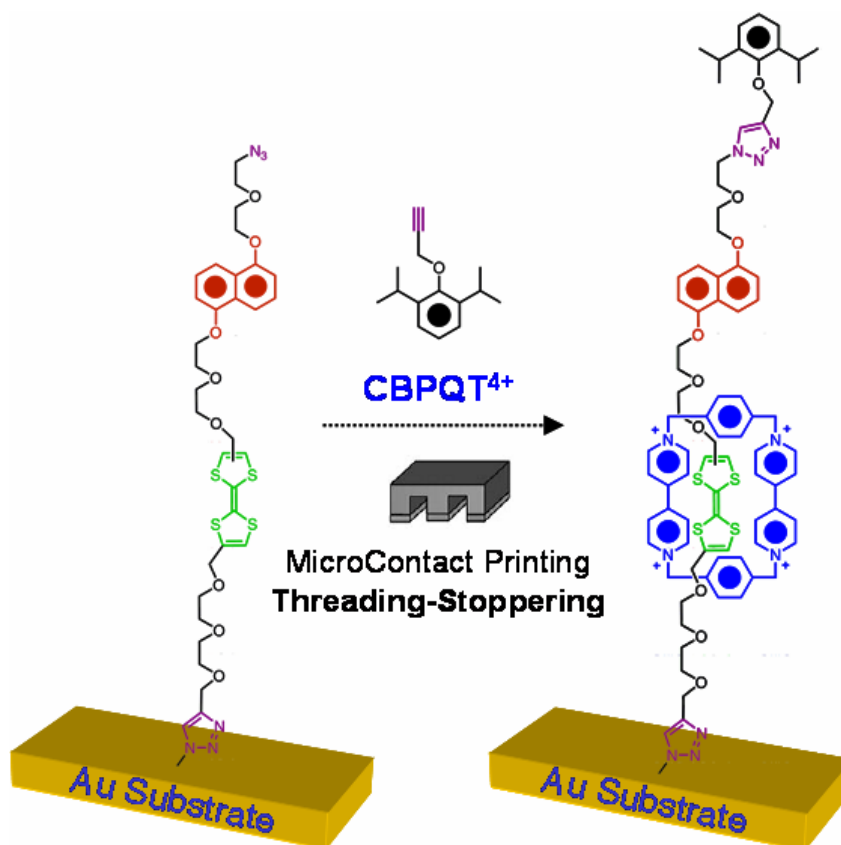
Figure 5.3. Schematic of proposed [2]rotaxane synthesis. The rotaxane backbone would first be covalently attached by μCP. The tetracationic cyclophane ring (CBPQT^{4+}) and the stopper would be also sequentially stamped, forming the complete [2]rotaxane on the electrode surface.

This proposed synthesis would allow for the rapid fabrication of both the molecule and device simultaneously. This process would be extremely fast, be high yielding, and generate little waste. Unlike the Langmuir-Blodgett technique, the monolayer would be covalently attached to the surface and also could be patterned into the desired device geometry. Advances in the nanoimprint lithography of nanowires[19] would provide a complement to this technology and be an attractive method for the high-throughput generation of novel nanoscale and molecule-based electronic circuits.

5.1.2 Organization of the chapter

This chapter describes the work done on developing μCP methods for the Cu^I-catalyzed azide-alkyne cycloaddition (CuAAC) reaction on Au and Si substrates. Because alkanethiol monolayers on Au are the best characterized SAM system,[20] the majority of the results were obtained using these substrates. μCP was shown to work using both homogeneous and heterogeneous Cu catalysts. The use of the heterogeneous catalyst for μCP was a novel result and its kinetics and mechanism were explored in detail.

In the next two sections, the stamping process and the surface characterization experimental methods are described. Then, the results of the surface characterization are discussed, followed by discussions of the kinetics of the stamping process using the homogeneous and heterogeneous stamps and the mechanism for μCP using the heterogeneous catalyst. Lastly, the generation of azide-terminated silicon surfaces is described, along with preliminary stamping results.

5.2   Generation of azide-terminated monolayers on Au

Mixed monolayers consisting of 50% azide termination and 50% methyl termination were prepared by immersing Au substrates into a 1 mM solution of 50% octanethiol and 50% 1-azido-11-undecanethiol in ethanol. Au surfaces were prepared by depositing 15/150 nm Ti/Au on clean, 4-inch Si(100) wafers. The wafers were cleaved into 1.5×1.5 cm^2 pieces and cleaned via a one minute soak in hot acid piranha (3:1 H_2SO_4: 30% H_2O_2), followed by a 15 second immersion in H_2O and a 15 second immersion in concentrated HCl at room temperature. The pieces were then rinsed with DI H_2O and EtOH, and were immediately placed in the thiol solution for 16–36 hours. The reaction was protected from light to prevent photo-oxidation of the thiols.[21] The Au substrates were then removed from the thiol solution, rinsed with EtOH, and dried with N_2. The azide-terminated Au samples can be stored, protected from light, for a few weeks.

5.3   CuAAC reaction conditions in solution and in stamping

The Cu^I-catalyzed azide-alkyne cycloaddition (CuAAC) was used to covalently attach ferrocene and other molecules to the Au surfaces. The CuAAC reaction on the Au surface in solution and using the stamps were compared. Here, the experimental conditions for each reaction are presented.

5.3.1 Solution CuAAC conditions

For the solution-based reaction, the 50% azide-terminated Au substrates were immersed in a 1–10 mM solution of 1:0.1:0.2 molar equivalents of ferrocene alkyne, $CuSO_4 \cdot 5H_2O$, and L-ascorbic acid in DMF. The reaction was protected from light and placed on a rocking platform to gently stir the reagents. Once the reaction was stopped, the Au samples were placed in fresh DMF and sonicated for 10 minutes, then rinsed with methanol and dried with N_2.

5.3.2 Microcontact printing CuAAC conditions using the homogeneous catalyst

For the CuAAC reaction using microcontact printing and an ink-based catalyst, referred to as *HomoCat*, polydimethylsiloxane (PDMS) elastomer stamps were first fabricated. PDMS was molded over either a flat or patterned 4-inch Si wafer. To prepare the Si wafer, it was first cleaned using hot acid piranha for ~ 15 minutes, rinsed in DI H_2O and dried with N_2. The wafer surface was rendered hydrophobic by exposing it to trimethylchlorosilane (TMCS) vapor for ~ 15 minutes. Afterwards, the surface was rinsed with H_2O and dried. The wafer was placed in a foil-covered shallow crystallizing dish and the edges were taped down to prevent PDMS from leaking under the wafer.

A 10:1 wt:wt mixture of PDMS-Sylgard Silicone Elastomer 184 and Sylgard Curing Agent 184 (Dow Corning Corp., Midland, MI) was mixed by hand and added to the crystallizing dish. The dish with the PDMS was degassed under reduced pressure for ~ 1 hour to remove trapped air bubbles in the PDMS and then heated to 60°C for a minimum of 1 hour to cure the PDMS. The cured PDMS was then carefully peeled from the Si wafer and diced into 1.5×1.5 cm^2 pieces.

The stamp ink consisted of three solutions mixed immediately prior to stamping: a 5 mM solution of the alkyne molecule in acetonitrile (ACN), and 1 mM solutions of $CuSO_4 \cdot 5H_2O$ and ascorbic acid in ethanol (EtOH). Prior to applying the ink, the PDMS pieces were oxidized using O_2 plasma (50 W, 10 seconds) to increase the ink wettability on the surface. The oxidized stamps were immediately placed in H_2O until needed. The stamps were soaked in ACN for ~ 30 seconds and then placed flat-side-up and dried with N_2. Several drops of the alkyne solution were added to the stamp until the surface was covered. Approximately 2 drops each of the ascorbic acid and the $CuSO_4 \cdot 5H_2O$ solutions were added and the stamp was gently rocked to mix the solutions. The ink solvent was allowed to evaporate (this process takes ~ 15 minutes in a chemical hood with the sash down). Once the solvent was gone, the stamp was gently placed into contact with the azide-terminated Au surface. A ~ 40 g weight was added to the stamp to ensure complete contact with the Au surface. Once the stamping was complete, the stamp was removed and the Au substrate was rinsed with EtOH and dried with N_2.

5.3.3 Microcontact printing CuAAC conditions using the heterogeneous catalyst

In this technique, referred to as *StampCat*, the ascorbic acid solution is eliminated and the $CuSO_4 \cdot 5H_2O$ in the ink solution is replaced by coating the PDMS stamp with a thin layer of Cu. After the PDMS stamp was made but before it was diced into smaller pieces, 10/50 nm of Ti/Cu was deposited onto the flat or patterned surface by electron beam evaporation. The Cu-coated PDMS stamp was then diced into pieces and used without performing the plasma oxidation step. Several drops of the 5 mM solution of the alkyne molecule were added to the Cu-coated surface and allowed to evaporate. The rest

of the stamping process was identical to that described above. In addition to Cu, Pt-coated PDMS stamps were also fabricated and used as a control.

5.4   Surface characterization experimental procedures

All functionalized surfaces were characterized using X-ray photoelectron spectroscopy (XPS), contact angle goniometry, infrared (IR) spectroscopy, frictional force microscopy (FFM), and electrochemical measurements. In this section, the experimental procedure for each characterization method is described.

5.4.1   XPS measurements

XP spectra were collected by a co-worker in a ultrahigh-vacuum chamber using an M-probe spectrometer (VG Instruments) as described previously.[22, 23] Measurements were taken from the center of each sample at room temperature. Monochromatic X-rays of energy 1486.6 eV from the Al Kα line were incident at 35° from the sample surface. Emitted photoelectrons were collected by a hemispherical analyzer located 35° from the sample surface. Data was collected using ESCA-2000 software.

Survey scans were collected in scanned mode from 0 to 1000 eV binding energy. High resolution spectra were collected in unscanned mode in the C 1s (282–289 BeV), F 1s (680–696 BeV), Br 3d (68–74 BeV), N 1s (396–410 BeV), Si 2p (97–106 BeV), Cl 2s (265–275 BeV), Cl 2p (195–205 BeV), and Fe 2p (700–730 BeV) regions.

5.4.2   Contact angle measurements

The sessile contact angle of water was measured using an NRL C.A. Goniometer Model #100-00 (Rame-Hart, Inc.) at room temperature. Each drop had a volume of ~ 1 µL and was applied to the surface using a syringe needle. Before every measurement, the sample platform was adjusted until there was no tilt in any direction. Typically, three drops per sample were measured and both the left and right contact angles were recorded and averaged.   After the contact angles were measured, samples were rinsed with methanol and dried with N_2.

5.4.3   Infrared spectroscopy measurements

External reflectance infrared spectra were collected using a Vertex 70 FT-IR spectrometer (Bruker Optics, Inc.) equipped with a liquid-N_2-cooled MCT detector and an AutoSeagull accessory (Harrick Scientific Products, Inc.). Samples were probed at a grazing angle of 85° with p-polarized light. Once the samples were loaded, the sample chamber was purged with dry air for approximately 30 minutes. Spectra were collected from 400 to 5000 cm^{-1} using 128 scans with a resolution of 4 cm^{-1}. A background spectrum was obtained from a freshly cleaned Au substrate and was subtracted from the spectra of functionalized surfaces. Spectra was baseline corrected using the concave rubberband method (25 iterations, excludes CO_2 bands, 256 baseline points).

5.4.4   Frictional force microscopy measurements

FFM measurements were made using a Multimode Nanoscope IIIA (Veeco Instruments, Santa Barbara, CA) atomic force microscope in contact mode. The scan

angle was set to 90° to maximize the friction signal. Topography was measured in trace mode and friction in retrace mode. General purpose, oxide-sharpened silicon nitride probe tips were used (NP-S). The best friction images were obtained using scan rates of approximately 1–2 Hz.

5.4.5 Electrochemical measurements

Cyclic voltammetry (CV) measurements were performed using a VMP Multi-Potentiostat (Princeton Applied Research, Oak Ridge, TN). Before each set of measurements, Ar gas was bubbled in the electrolyte, 1 M perchloric acid, for ~ 30 minutes. The sample was loaded into a custom-made, Teflon cell that held approximately 1 mL of electrolyte. The area of the sample surface exposed in the electrochemical cell was 78.6 mm^2. The counter electrode, a Pt wire, was cleaned by exposing it to a flame for ~ 10 seconds. Both the counter electrode and a Ag/AgCl reference electrode were immersed in the electrolyte. Electrical contact was made to the Au substrate (the working electrode) outside of the electrochemical cell. Cyclic voltammagrams were obtained for scan rates of 50–700 mV/s. Before a new sample was loaded, the Teflon cell was sonicated in H_2O for ~ 30 seconds, rinsed with DI H_2, and dried with N_2. The counter and reference electrodes were also rinsed with DI H_2O between samples. After the CV measurements were made, the samples were rinsed with MeOH and dried with N_2.

It was observed that noisy CV data could almost always be eliminated by re-loading the sample into the electrochemical cell and adding fresh electrolyte. The largest source of noise seemed to be from improperly loaded samples.

5.5   µCP results using homogeneous and heterogeneous catalysts

The µCP method was used to covalently attach **3** to the azide-terminated monolayers (50% **1** and 50% **2**) on Au (Figure 5.2).   For the homogenous catalyst (*HomoCat*), the Cu^I catalyst was generated in the ink solution by the reaction of $CuSO_4 \cdot 5H_2O$ and ascorbic acid. Heterogeneous catalysis (*StampCat*) was achieved by coating the PDMS stamp with a 50 nm Cu layer. Both methods did facilitate the formation of the 1,2,3-triazole ring. The

Figure 5.4. Molecular structures from the azido-terminated monolayers (50% **1** and 50% **2**) and the stamp inks: ferrocene alkyne (**3**) and pentafluorophenylether alkyne (**4**)

reaction was confirmed using contact angle goniometry, IR spectroscopy, XPS, FFM, and electrochemistry.

5.5.1 Contact angles

The contact angle measurements were taken on azide-terminated surfaces for both the *HomoCat* and *StampCat* techniques. The mixed monolayer of **1** and **2** yielded a contact angle of 77°, which is in agreement with previous reports.[24] The covalent attachment of **3**—whether via solution-based, *StampCat*, or *HomoCat* methods—caused an expected reduction in contact angle to approximately 70°. To show generality of the reaction, the *StampCat* technique was also performed using **4** as the ink. The fluorine

groups caused the contact angle to increase as expected. The summary of the contact angles are presented in Table 5.1.

Table 5.1. Contact angle measurements for various modified Au surfaces

Surface	Method	Molecule	H_2O Contact Angle (°)
Au	–	–	56.5 +/- 1.5
50% N_3 on Au	–	–	76.5 +/- 1.7
50% N_3 on Au	*Solution-Based*	**3**	72.6 +/- 3.0
50% N_3 on Au	*HomoCat*	**3**	68.5 +/- 5.3
50% N_3 on Au	*StampCat*	**3**	73.5 +/- 3.4
50% N_3 on Au	*StampCat*	**4**	80.3 +/- 3.6

5.5.2 Grazing angle infrared spectroscopy

IR spectroscopy also confirmed the CuAAC reaction. Figure 5.5A shows the stacked grazing angle IR spectra for the azide-terminated surface and for **3** attached via *HomoCat*, *StampCat*, and solution-based reactions. Note that the CO_2 bands were removed from the spectra.

Figure 5.5B shows the region between 3000–2000 cm^{-1}. The peaks between 2800 and 2900 cm^{-1} are indicative of methylene stretches. Major peaks that appear in each spectra are located at 2867 cm^{-1} and 2932 cm^{-1}, which correspond to the methylene symmetric and asymmetric stretches, respectively.[25] The azide asymmetric stretch appears prominently in the azide-terminated monolayer spectra at 2104 cm^{-1}, reduces significantly in the *HomoCat* and *StampCat* spectra, and disappears completely in the solution-based reaction spectra.

Figure 5.5C shows the IR spectra in the carbonyl region between 1600 and 1800 cm^{-1}. The azide-terminated surface is relatively flat in this region but the ferrocene-terminated surfaces show a large peak at around 1713 cm^{-1}. This peak was absent in the

StampCat reaction with **4**, which suggests this peak may be due to the carbonyl stretch associated with the ester in **3**.

Lastly, figure 5.5D shows the spectra of the *StampCat* reaction with **4** and the azide-terminated surface. The spectrum of 4 has a large peak at 1625 cm^{-1} that was not present in the surfaces containing **3**. This is attributed to the C-F stretches on the phenyl group.[26]
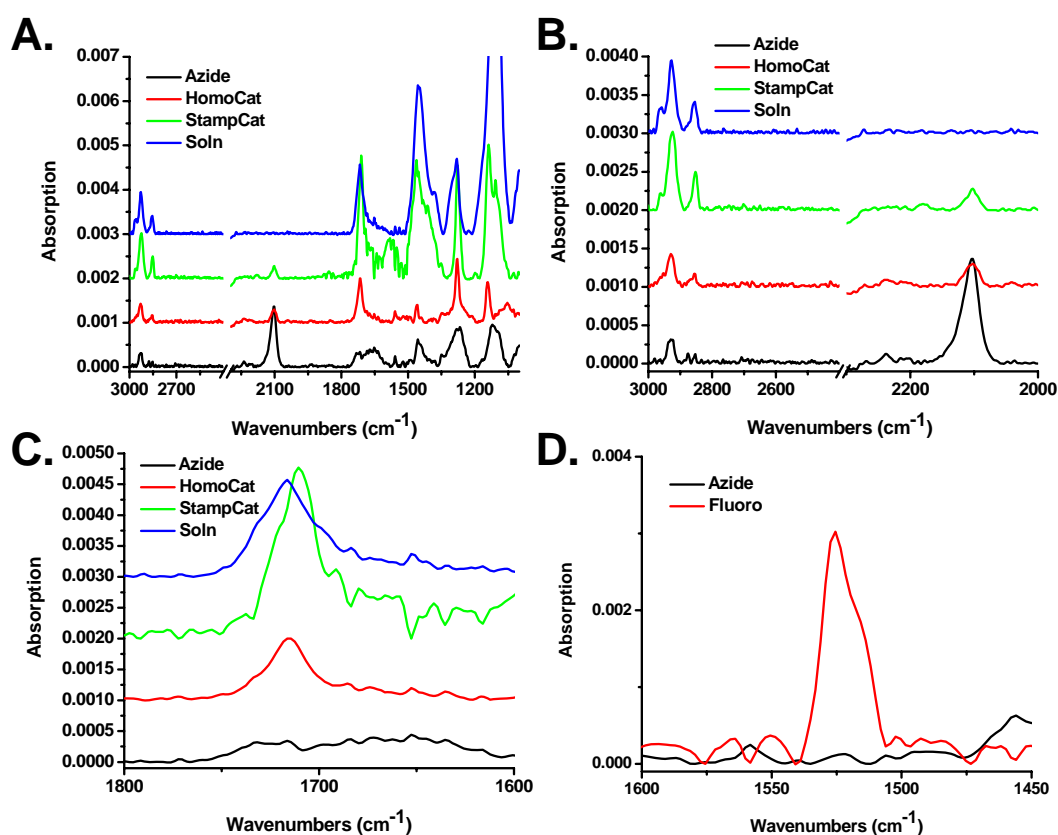
Figure 5.5. Grazing angle IR spectra of azide-terminated and stamped surfaces. **A.** Stacked survey spectra of azide-terminated surface (black) and *HomoCat* (red), *StampCat* (green), and solution-based (blue) reaction with **3**. **B.** Close-up of methylene and azide bands. **C.** Close-up of carbonyl bands. **D.** Close-up spectrum of **4** attached to surface via the *CatStamp* method, showing C-F stretches.

5.5.3 X-ray photoelectron spectroscopy

XPS elucidates the elemental composition on surfaces and is a powerful surface characterization technique. The XPS spectra for surfaces bound with azide, **3,** and **4** are presented in Figure 5.6.
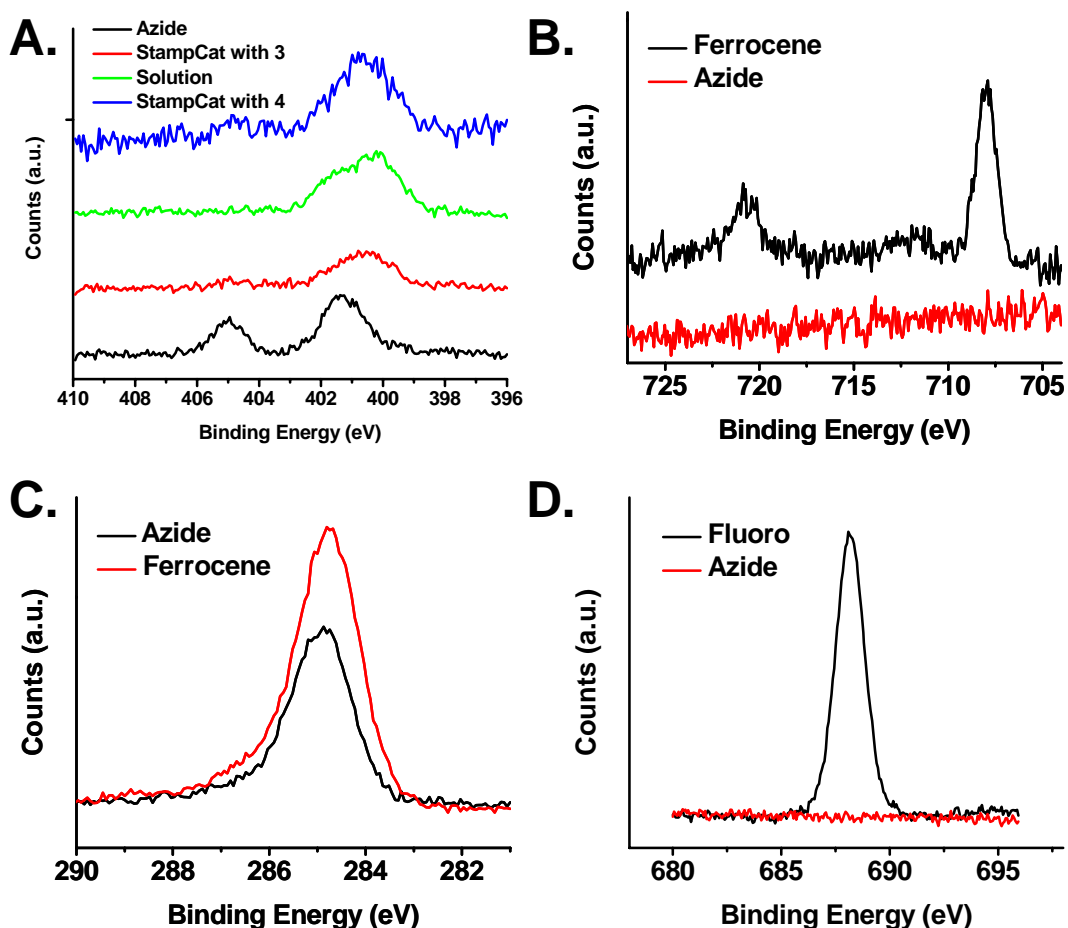
Figure 5.6. XPS data of azide-, **3**-, and **4**-terminated surfaces. **A.** Spectra of azide-, **3**-, and **4**-termated surfaces in N 1s region. **B.** Spectra of same surfaces in Fe 2p region. **C.** Spectra of same surfaces in C 1s region. **D.** Spectra of azide- and **4**-terminated species in F 1s region

Figure 5.6A shows the high-resolution XPS spectra of the azide-, **3**-, and **4**-terminated surfaces in the nitrogen 1s region. The azide spectrum shows the

characteristic two peaks at 400 and 405 eV. The higher peak is indicative of the electron-deficient nitrogen in the azide group. After the solution-based (green curve) and *StampCat* reactions with **3** (red curve) and the *StampCat* reaction with **4** (blue curve), the higher energy peak disappears and the peak at 400 eV broadens. This is suggestive of the chemically distinct nitrogen atoms in the 1,2,3-triazole.

Correlated with the disappearance of the azide group, an iron signal appears in the Fe 2p region (Figure 5.6B). The peak at 720 eV is from the $2p_{1/2}$ electrons and the peak at 708 eV is $2p_{3/2}$ electrons. The corresponding azide-terminated surface shows only the noise level in this region. Additionally, the carbon 1s peak shows an increase in peak area after the attachment of **3** to the surface (Figure 5.6C). Lastly, the attachment of **4** corresponded to the appearance of a large peak in the fluorine 1s region (Figure 5.6D). The peak, centered at 688 eV is indicative of the C-F bond.

5.5.4 Frictional force microscopy

Frictional force microscopy (FFM) is the best tool for characterizing surfaces that are patterned since it yields information about the surface with atomic resolution.[27] Like EFM, which is described in Chapter 3, FFM (also known as lateral force microscopy) is a variant of AFM. In this technique, the AFM is operated in contact mode but the cantilever scans the surface perpendicular to the cantilever's major axis. This makes the cantilever very sensitive to tip-surface interactions. A high-friction or low-friction surface will torque the cantilever to different extents, generating a friction map. Figure 5.7A shows a schematic of an AFM cantilever scanning over a low-friction area (1) and a high-friction area (2).

Silicon wafers patterned with 12 × 9 μm dots or 4.25 μm stripes using EBL was used to mold PDMS stamps to study pattern transfer using *StampCat*. Cu was deposited onto the patterned stamps and the stamping was performed in the same manner as for the flat PDMS stamps.

A.

B.

C.

D.
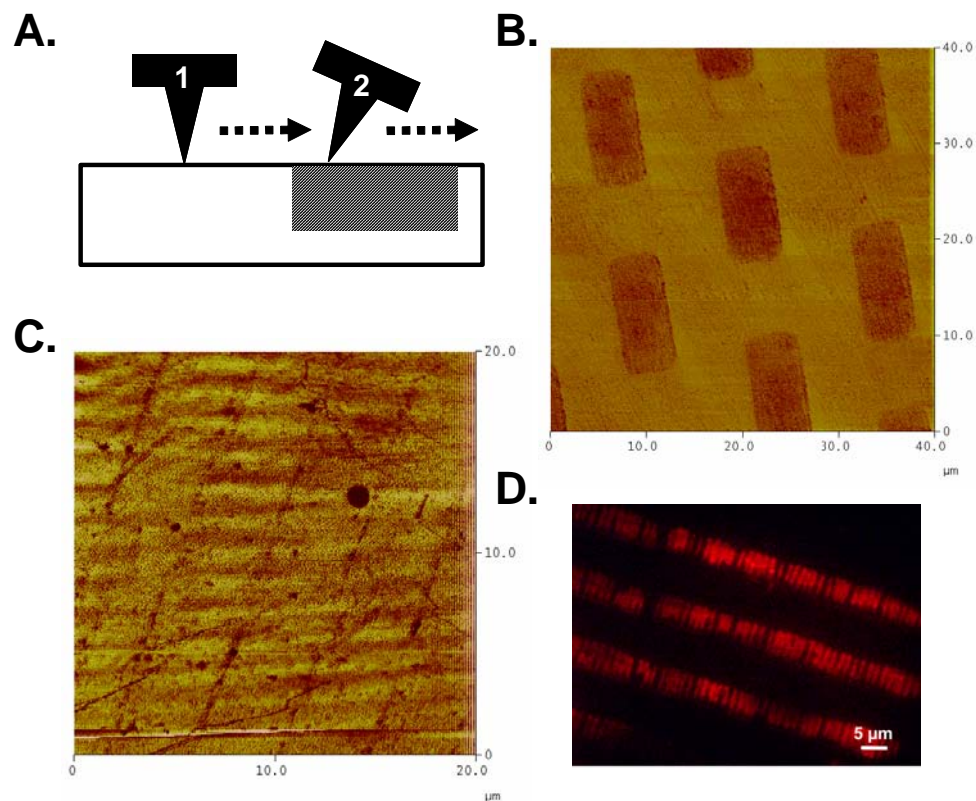
Figure 5.7. FFM and fluorescence characterization of patterned surfaces. **A.** Side-view schematic of AFM tip interaction with a surface containing a low friction area (**1**) and a high friction area (**2**). **B.** and **C.** FFM image of **3** patterned on surface by the *CatStamp* technique. **D.** Fluorescence image of rhodamine patterned on glass, showing that small defects were transferred from the stamp

Figure 5.7B shows the frictional image of the patterned Au monolayer using the stamp patterned with dots. After one hour of stamp time, the dots pattern did not diffuse or distort. This suggests that the nature of the catalyst is truly heterogeneous and that the reaction only occurs where the stamp is in intimate contact with the surface.

Figure 5.7C also provided evidence of this conclusion. The friction image recorded a series of thin lines for the pattern that contained large bars. At first this was attributed to a faulty FFM signal. However, the stamp itself was imaged and the bars were shown to be distorted so that the edges curled up. The pattern transfer in Figure 5.7C was a result of just the edges of the stamp making contact with the surface. Again, no pattern diffusion was evident. This was also observed when patterning rhodamine on glass substrates (experiment was performed by Dorota Rozkiewicz). Small breaks on the patterned bars (Figure 5.7D) were observed both from the fluorescence image of the surface and on the stamp itself.

5.5.5 Electrochemistry

Figure 5.8A and 5.8C shows the cyclic voltammogram of **3** patterned by the *HomoCat* and *StampCat* techniques for various scan rates, υ. The oxidation and reduction of ferrocene is a one-electron process, as evidenced by the single oxidation and reduction peaks centered at ~ 0.5 V. The magnitudes of the oxidation and reduction peak currents are equal, indicating the reaction is Nernstian (reversible). A plot of the peak oxidation current as a function of υ reveals a linear relationship for both *HomoCat* and *StampCat* (Figure 5.8B and 5.8C inset). The correlation coefficients, *R*, for the *HomoCat* and *StampCat* curves were 0.99995 and 0.99998, respectively. This relationship indicates that **3** was fully adsorbed on the surface. For species that can diffuse through the cell, the peak current will have a $\upsilon^{1/2}$ dependence.[28]

Two controls were also measured. The first control was an azide-terminated Au substrate stamped with a bare PDMS stamp and the second control used a Pt-coated

PDMS stamp (prepared in an analogous method to the Cu-coated PDMS stamp). Both controls used an ink solution of **3** with no added Cu catalyst. The electrochemistry indicated that no reaction occurred (Figure 5.8D) for either control stamp, providing evidence that the Cu metal is indeed catalyzing the CuAAC reaction.
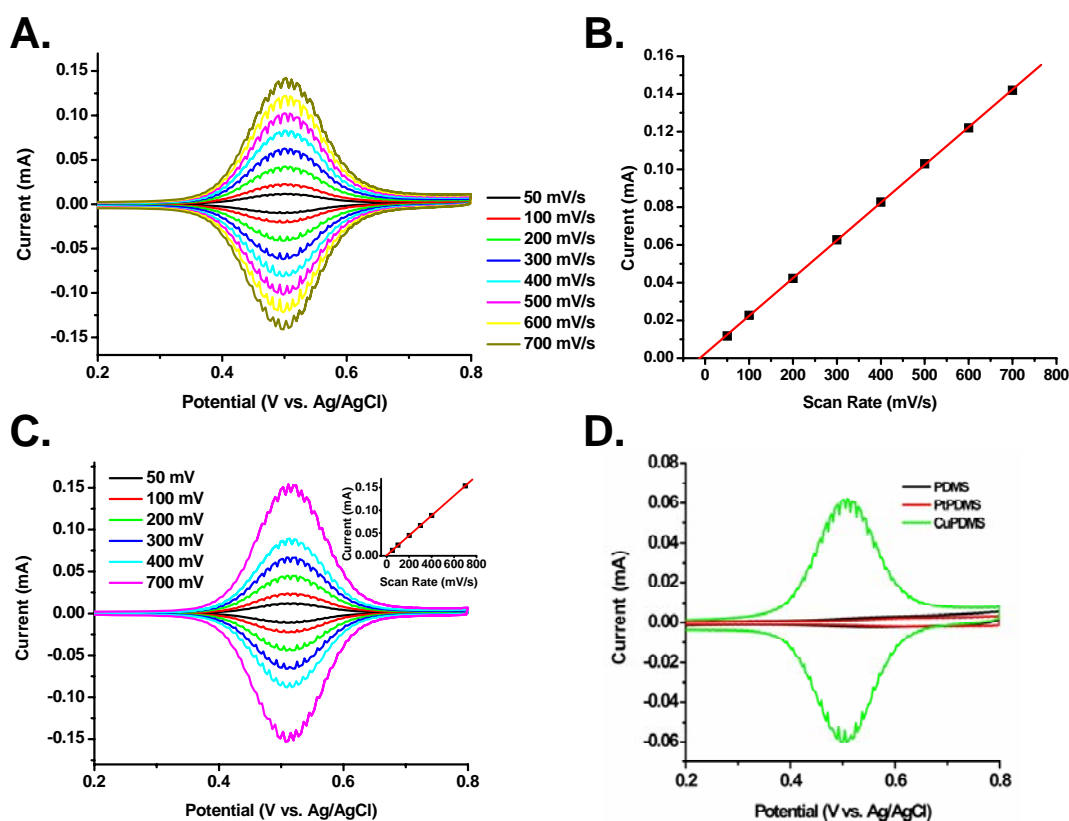
Figure 5.8. Electrochemistry of **3** patterned using the *HomoCat* and *StampCat* methods. **A.** Cyclic voltammogram of **3** stamped via *HomoCat* for various scan rates. **B.** Oxidation peak current as a function of scan rate, showing a linear relationship. C. Cyclic voltammogram of **3** stamped via *StampCat* for various scan rates. **Inset:** Oxidation peak current versus scan rate. **D.** Cyclic voltammetry of surfaces stamped with a Pt-coated PDMS (red trace) and bare PDMS (black trace) stamp with no added catalyst in comparison with a Cu-coated PDMS stamp (green trace).

There has been published evidence of the azide-alkyne cycloaddition occurring without a catalyst using μCP.[5, 6] It is hard to explain the cause of this discrepancy. AFM and fluorescence microscopy were used extensively in these studies to show pattern

transfer from the stamp to the surface. It could be that these characterization tools, neither of which are able to quantify surface coverage, are much more sensitive to a very low surface coverage of molecules. The resolution of florescence microscopy is several hundred nanometers[29] and so a strong fluorescence image may be present even for a few molecules. Similarly for AFM, a height difference may be observable even for a sparse packing density of molecules.

Another explanation is that the azide-alkyne cycloaddition can proceed without the Cu catalyst in elevated temperatures.[30] Although not explicitly mentioned in the published reports, heating the substrates during the stamping process was done occasionally.[31] For this study, it was not necessary to eliminate the catalyst and there was no further attempt to explore these different observations.

5.6   Stamp kinetics comparison

The advantage of doing electrochemical measurements is that they can be used to quantitate the surface coverage of the bound electroactive species. The area under the oxidation peak can be used to determine the amount of charge involved in the oxidation. Since the oxidation of ferrocene is a one-electron process, the amount of charge is equal to the amount of **3** bound to the substrate.

Using scientific plotting software, the oxidation peak over the second scan for each voltammogram was baseline corrected and the area was determined numerically

using the trapezoidal rule. The area in units of V·A is divided by the scan rate (in V/s) to determine the amount of charge, Q. The charge in Coulombs is converted to the amount of electrons by using the conversion factor, 6.24×10^{24} electrons/C. The number of electrons in the oxidation process is also equal to the number of molecules involved (for a one-electron process). By knowing the electrochemistry cell area (in this case, 0.78 cm^2), the number of molecules per unit area can be determined. Based on published results,[24] the amount of azide groups per unit area for a mixed monolayer of 50% **1** and 50% **2** on Au(111) is ~ 2.1×10^{14} cm^{-2} (assuming 45% azide coverage). A ratio of the calculated amount of **3** to this value yields the percent coverage.

Figure 5.9 shows the kinetics of the covalent attachment of **3** using the *HomoCat* and *StampCat* methods. Both reactions go to completion but the *HomoCat* reaction rate is faster than *StampCat* (30 minutes versus 60 minutes to completion). The relationship between percent azide consumed and time shows different rate laws for the two reactions.

The *StampCat* kinetics follow a zero-order reaction rate, as evidenced by the linear relationship between the percent azide consumed and time. The half-life of the reaction is ~ 30 minutes. Reactions involving heterogeneous catalysts can usually be described by using the Langmuir-Henshelwood or Eley-Rideal mechanisms.[32] The Langmuir-Henshelwood mechanism describes a mechanism in which two
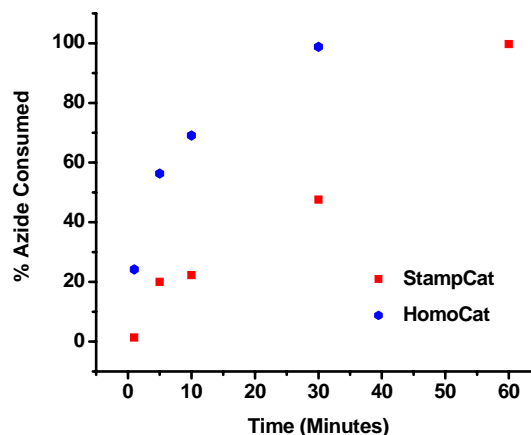
Figure 5.9. Kinetics plot of the StampCat and HomoCat techniques with **3**

reactants, A and B, adsorb onto a surface (typically the heterogeneous catalyst), diffuse and react once in close proximity. This mechanism is not likely since the azide groups are immobilized to the Au substrate. The Eley-Rideal mechanism describes a scenario where only one reactant adsorbs onto the surface. The reactant desorbs when it is in close proximity to the other reactant (which does not adsorb onto the surface). At high concentrations of the adsorbed reactant, the reaction becomes zero order.[33] Since the *StampCat* reaction is solvent-free, it has an extremely high concentration of the alkyne reactant. Although Eley-Rideal mechanisms are rare, the unique nature of having two immobilized reactants (the azide groups and the Cu catalyst) makes this the most likely mechanism.

It appears that the *HomoCat* kinetics follow a first-order exponential growth function. The half-life of the reaction is ~ 5 minutes. It is likely that because the alkyne is present in excess that the mechanism would follow a pseudo-first-order rate law. However, because there were no error bars on the data, it was not possible to estimate a rate constant, k, from the plot. More data points would most likely lead to a confirmation of the pseudo-first-order rate law.

5.7   The *StampCat* mechanism

The azide-alkyne cycloaddition to 1,4-disubstituted 1,2,3-triazoles is catalyzed by Cu in its +1 oxidation state.[34, 35] This reaction occurs via a step-wise mechanism. First, a Cu^I acetylide species is generated via a π complex which leads to the insertion of Cu onto the terminal end of the alkyne.[36] A ligation sequence begins where the azide's electron-rich nitrogen binds to the Cu^I, followed by a ring closure by the terminal nitrogen and the secondary carbon in the alkyne group.[34] DFT calculations have shown that the addition of the Cu^I ions lowers the activation energy of this process by as much as 11 kcal/mol and the reaction rate occurs up to 10^7 times as fast as the uncatalyzed reaction.[36]

Cu^I salts, such as CuI, can be used directly. However, undesired side reactions can limit the use of these salts.[35] Typically, Cu^{II} (such as $CuSO_4 \cdot 5H_2O$) is added and reduced to the Cu^I state *in situ* using a reducing agent. There have also been reports of Cu metal, in the form of turnings,[34] Cu/C,[37] and Cu clusters,[38] catalyzing this reaction. The removal of Cu from these reactions typically requires simple filtration, which makes this an attractive alternative to solution-based catalysts. However, the use of Cu^0 in CuAAC reactions is still rare (possibly due to the slower reaction rates observed for Cu^0 systems) and there have been few reports on the mechanism of the catalysis.

Studies have shown that for CuAAC reactions using high surface area Cu^0 catalysts, there was no evidence of Cu atoms or ions leaching into the reaction.[38, 39] In one experiment, the conversion to the triazole product between prop-2-yn-1-ol and benzyl azide was monitored as a function of time. When the catalyst, Cu powder, was filtered out of solution, no evidence of any further conversion was observed. The powder was

added back to the reaction and the reaction proceeded again at the same rate. This observation is consistent with the evidence in this study where after 1 hour of stamp time using a patterned stamp, no evidence of pattern diffusion was observed (see Section 5.5.4).

Since free Cu^I is not responsible for catalyzing the cycloaddition, it has been proposed that CuO and Cu_2O present on the surface of the Cu metal are responsible.[37, 40] An experiment was performed that examined the reusability of Cu-coated PDMS stamps. The stamping procedure was performed using **3** as the ink on the azide-terminated Au surfaces as described earlier. After 15 minutes of stamp time, the stamp was carefully removed from the substrate and the ink was reapplied. Three more substrates were stamped using the original stamp and their ferrocene concentration was measured using electrochemistry (Figure 5.10A).
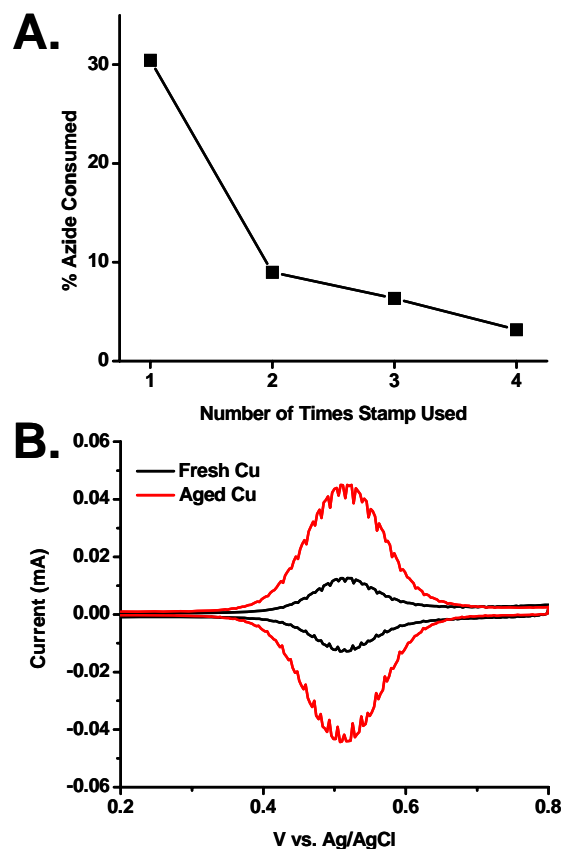
Figure 5.10. Elucidating the mechanism of *StampCat* using electrochemistry. **A.** Percent azide consumed as a function of repeated stamp use. **B.** Cyclic voltammograms of **3** patterned using *StampCat* using a freshly deposited Cu (black trace) and two day old Cu (red trace)

The stamp reusability results suggest an immediate loss of catalytic behavior after one use. The subsequent stampings show significantly smaller decreases. The structure

of the native oxide on Cu consists of an inner layer of Cu_2O and an outer layer of CuO. The growth of CuO is very slow and for freshly deposited Cu films at room temperature, the oxide would predominantly be Cu_2O.[41] After the first stamping, the majority of the Cu_2O on the surface of the stamp is somehow depleted from the stamp. This is consistent with the observation of an increase of the ink wettability on the surface after the first stamping (the ink wets Cu^0 much better than Cu_2O). The other reactions were limited by the regrowth rate of the Cu_2O between stamping. Similar observations were reported reusing Cu nanoclusters to catalyze the cross-coupling of alkynes and aryl halides.[39] After three uses, the nanoclusters could not catalyze the reaction to completion after 24 hours. Further evidence was provided by comparing the reaction rates of stamps used immediately after the Cu deposition versus after a two day delay. Older stamps displayed a higher catalytic ability (Figure 5.10B) for the same stamping time (~ 1 hour).

Due to the limited wettability of the deposited metal on PDMS and the flexible nature of the stamp, the Cu coating on the PDMS stamps was noticeably cracked on the microscale. It is likely that the deposited Cu also has significant surface roughness and contains many vacancies and dislocations. Cu films of this quality grow native oxide significantly quicker than higher quality films.[41] It is believed that this only helps the catalytic nature of the stamp. For other heterogeneous Cu catalysts, a higher surface area and more irregular consistency results in an enhancement of reaction rate.[38] Based on the evidence from this study and others, it is believed that the initial Cu^I acetylide species is generated from the Cu_2O present on the Cu stamp's surface.

5.8   µCP on silicon surfaces

Thiol monolayers on Au substrates, while well characterized, have limited utility. The dominant material for electronics is silicon and transferring the µCP process to silicon substrates would enable many technologies. For instance, the [2]rotaxane synthesis would need to be performed on Si substrates. The following sections describe two methodologies for generating azide-terminated silicon surfaces and preliminary stamping results on each.

5.8.1   Generation of azide-terminated alkane monolayers on Si(111)

One appealing chemistry for producing azide-terminated Si(111) surfaces is the hydrosilylation reaction using a diacyl peroxide as a radical initiator.[42, 43] In this reaction, a linear alkane molecule containing a alkene or alkyne termination is inserted into the silicon-hydride group of a hydrogen-terminated Si surface.[44] This reaction proceeds via a radical mechanism in which the diacyl peroxide undergoes a homolytic cleavage and subsequent decomposition to form an alkyl radical. This radical is transferred to the Si surface where it can react with the unsaturated group in the alkane molecule. This process continues until a complete monolayer is generated.

This chemistry is attractive because it forms densely packed, high-quality monolayers that are very resistant to oxidation. Chidsey et al. reported that hexadecyl monolayers synthesized using this chemistry were resistant to oxidation when exposed to boiling $CHCl_3$ (2 hours), boiling H_2O (7 hours), and air (11 weeks).[43] In comparison, hydrogen-terminated Si(111) and methyl-terminated surfaces prepared using

electrochemical anodization or the Lewis acid-mediated reduction of a terminal alkene

form oxide within minutes of air exposure.[23] The high stability of the monolayers formed

via hydrosilylation is useful for applications that require the Si surface to be exposed to

air or aqueous environments, such as electronics and biological sensing.

The azide-terminated monolayers were generated by first forming chlorine-

terminated alkyl monolayers on the surface, followed by the SN_2 substitution of chlorine

to azide. To generate Si(111) surfaces, 1 cm^2 Si(111) pieces were first cleaned for 1 hour

in hot acid piranha (3:1 H_2SO_4: 30% H_2O_2), followed by 15 minutes in hot basic piranha

(30% NH_4OH: 30% H_2O_2) and an additional 30 minutes in acid piranha again. The

substrates were rinsed with DI H_2O after each cleaning step. Next, the Si pieces were

immersed in 40% NH_4F until the surfaces were covered in small bubbles (indicative of

hydrophobicity), ~ 5 minutes. The samples were rinsed in DI H_2O for 30 seconds, dried

with a N_2 stream and used immediately.

The hydrosilylation reaction was performed successfully using a 1:1 wt:wt ratio

of 1-chloro-11-undecene (Aldrich, 97%) and lauroyl peroxide (Luperox LP, Aldrich,

97%), as well as a 9:1 ratio. Chidsey reported that 90% of the monolayer will be derived from the alkene molecule, regardless of ratio. Both reagents were used without further purification. The alkene/peroxide mixture was placed in a round bottom flask
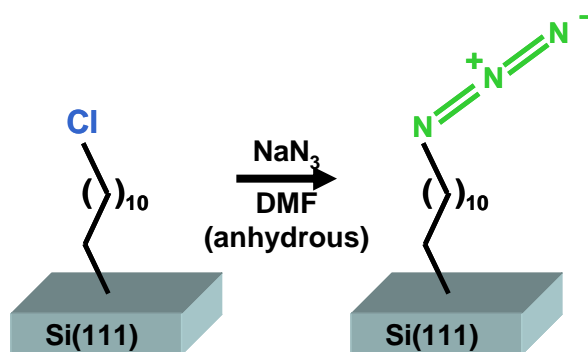
Figure 5.11. Schematic of azide-terminated monolayer on Si via hydrosilylation of 1-chloro-11-undecene and subsequent substitution to the azide

containing at least two necks, connected to a Shlenk line, and heated to 70°C under vacuum until the peroxide dissolved. The flask was backfilled with Ar and the hydrogen-terminated samples were carefully added. The flask was evacuated again, backfilled with Ar and heated to 100°C for 1 hour. Note, the reaction vessel must be vented to a mineral oil bubbler to reduce the risk of explosion! After the reaction was stopped, the samples were rinsed with EtOH and hexanes, sonicated twice for 5 minutes in $CHCl_3$, rinsed with EtOH and dried with N_2.

The azide substitution reaction (Figure 5.11) was performed in the glovebox to prevent surface oxidation. The chlorine-terminated samples were placed in vials containing a saturated solution of NaN_3 in anhydrous DMF. The vials were sealed with aluminum foil and placed on a hotplate set to 100°C for at least 16 hours. The samples were then rinsed with DMF and methanol, and dried.

5.8.2 Generation of direct azide-terminated silicon surfaces

An alternative method for generating azide-terminated Si surfaces is to form direct azide bonds to the surface Si atoms. This is a novel approach, developed by Peigen Cao in the Heath group, and has not been previously reported by other groups. Since the alkane spacer is eliminated, subsequent CuAAC reactions would generate interesting monolayers with better electrical contact to the substrate. This would have a large impact on chemical and biosensors, as well as molecular electronics.

The first step in generating azide-terminated Si surfaces is to form a high quality hydrogen-terminated surface. Si(111) wafers were cleaved into 1 cm^2 pieces and sonicated in methanol for 5 minutes. Teflon reaction beakers and sample tweezers were

cleaned by filling them with diluted basic piranha (1:1:4 NH₄OH: H₂O₂: H₂O) at 80 °C for 10 minutes. After rinsing the beakers out with DI H₂O, they were filled with a new solution of basic piranha. The samples were rinsed with water and placed in the basic piranha solution for 10 minutes at 80°C. Samples were removed from the basic piranha solution, rinsed with DI H₂O, and dried with N₂. It is important that the samples be completely dry. The samples were then immersed in NH₄F at room temperature for at least 15 minutes. The samples were then rinsed with DI H₂O (the samples should be very hydrophobic at this point) and dried with N₂.

Next, the hydrogen atoms on the Si surface were replaced with chlorine atoms. The samples were loaded into a glove box containing an inert atmosphere for the chlorination reaction. A scant amount (~ 1 mg) of benzoyl peroxide, the reaction initiator, was added to large, glass test tubes. One substrate is added per test tube and several mL of a saturated solution PCl₅ in chlorobenzene was added. The test tubes were headed to 95°C for 45–50 minutes. The reaction can also be done at RT for ~ 5 hours to generate a smooth surface for STM measurements. Once the reaction is complete, the samples were rinsed with THF, followed by methanol (MeOH) and immediately used for the azide substitution reaction.

Several substitution reaction conditions were tried to generate azide surfaces from the chlorine-terminated surfaces with the highest surface coverage (Figure 5.12). Here, the
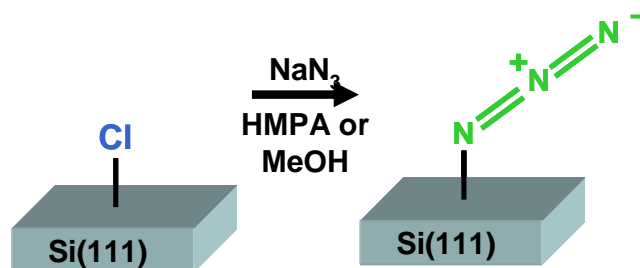
Figure 5.12. Schematic of synthesis of direct azide-termination on Si(111)

procedures that yielded surface coverages of ~ 30% and ~ 65% will be described here. For the lower coverage reaction, the freshly prepared, chlorinated Si samples were added to a saturated solution of sodium azide (NaN_3) in anhydrous methanol and left at room temperature overnight. For the high coverage reaction, an excess of CaH_2 was added to a vial of 99% Hexamethylphosphoramide (HMPA) for 1–2 days to remove water. The mixture was filtered using a 0.25 μm filter prior to the reaction. A large excess of NaN_3 was added to the filtered HMPA. Upon the addition of NaN_3, the solvent changed from yellow color to a dark orange. Chlorine-terminated samples were placed in the NaN_3 solution for 5 minutes at RT. Note that the NaN_3/HMPA mixture is photosensitive. For both reactions, the substrates were then removed, rinsed with copious amounts of tetrahydrofuran (THF) and methanol, and used immediately.

5.8.3 Stamping results on azide monolayers formed via hydrosilylation

XPS analysis confirmed that the SN_2 reaction to form the azide-terminated monolayers was successful. The spectra for both surfaces in Cl 2s region (Figure 5.13A) show the disappearance of the chlorine peak after the azide reaction. The chlorine 2p peak, located at 201 eV, also disappears after the azide reaction. At the same time, nitrogen peaks at 401 and 405 eV, characteristic of the azide group, appear. Additionally, the contact angle dropped from 99° to < 65° after the SN_2 reaction.

The ferrocene alkyne, **3**, was attached to the azide-terminated monolayers by *StampCat* and by the solution-based reaction, as described in Section 5.3. The reaction was successful for both reaction conditions. The XPS data in the nitrogen region show the disappearance of the peak at 405 eV and the broadening of the 401 eV, as expected

for the formation of the triazole ring (Figure 5.13B). The appearance of iron peaks are also observed for both reactions (Figure 5.13C). The contact angle of the surface from the solution-based reaction increased to 68°.
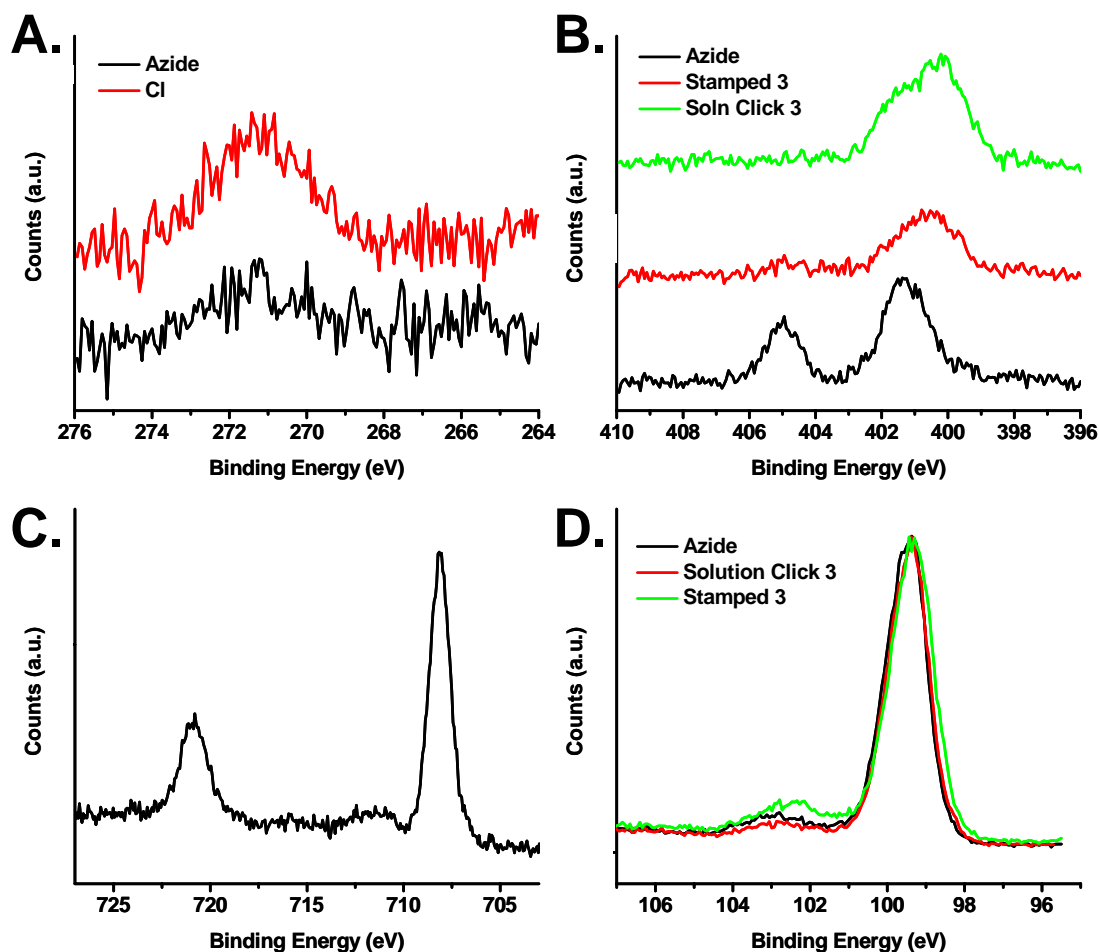
Figure 5.13. XPS data for CuAAC reactions on azide-terminated surfaces made via hydrosilylation. **A.** Stacked spectra of the chlorine- (red) and azide-terminated (black) surfaces in the C 2s region. **B.** Stacked spectra of the azide-terminated surface (black) and surface patterned with **3** via *StampCat* (red) and by solution-based CuAAC. **C.** Spectra of the solution-based reaction in the Fe 2p region. **D.** Spectra of the azide-terminated surface (black) and surfaces patterned with **3** via solution (red) and *StampCat* (green)

Because the monolayer on the surface contains 11 carbons, it was difficult to quantify monolayer surface coverage using the carbon 1s region. Instead, the ratio of the SiO_x peak (centered at 103 eV) to the Si 2p peak (centered at 99.5 eV), divided by the

normalization constant of 0.21, was used to determine the amount of surface atoms that were oxidized.[23, 45]

For the azide-terminated surfaces, the amount of surface Si atoms oxidized was ~ 0.3, which corresponds to ~ 70% monolayer surface coverage (Figure 5.13D). There was no further oxidation observed after the solution-based reaction. This is not surprising since the reaction was carried out in the glove box. The stamped surfaces, however, did show an increase in the SiO_x peak. The resulting surface coverage dropped to ~ 60%. The stamping was done outside of the glove box so the sample was exposed to ambient air for a few hours. Stamping inside of the glove box should eliminate any additional oxidation. Although the surface does not appear to be as robust as reported,[43] reaction conditions have not yet been extensively explored.

5.8.4 Stamping results on direct azide-terminated silicon

Several solution-based and stamping experiments were performed on the direct azide-terminated silicon surfaces. XPS and contact angle results indicated that the CuAAC reaction with **3** proceeded very poorly. Solution-based reactions were performed using several different solvents, including DMF, MeOH, acetonitrile, and HMPA. Reactions were also performed with 0.2 equivalents of tris-(benzyltriazolylmethyl)amine (TBTA), which strongly facilitates the formation of the 1,2,3-triazole and also inhibits oxygen reduction by the Cu catalyst.[24] The addition of TBTA did not have any effect. As a control, the same reaction conditions were used on a 50% azide-terminated monolayer on Au and XPS confirmed that the reaction went to completion. Other alkyne species were tried without success. Molecules that contained a carbonyl group next to

the alkyne group were tried in hopes that the carbonyl group's electron withdrawing nature would facilitate a Cu-free "click" reaction,[46] but no reproducible evidence of this reaction was observed.

Numerous stamping experiments were also performed. Cu-coated stamps were stamped onto freshly prepared, azide-terminated Si(100) and Si(111) substrates for 1 hour using **3** as the ink. Azide-terminated surfaces with both 30% and 70% coverage were used as substrates to see the effect of coverage and reaction efficiency. Again, no evidence was observed using XPS or contact angle measurements that the reaction occurred beyond a few percent conversion. These results are not surprising since the *StampCat* mechanism is not expected to be different from the solution-based reaction, which also failed. To facilitate the reaction, substrates were also heated to 40–50°C during the stamping with no effect. The XPS results suggested that not only does the reaction not proceed quantitatively, the azide-termination provides little protection from oxide growth, which occur within hours for Si(111) surfaces and minutes for Si(100) surfaces.

Since the azide-terminated surface is so fascinating, it is important to understand why the CuAAC reaction does not proceed readily and if conditions exist that would make it favorable. It is interesting that, regardless of azide surface coverage, the reaction fails. This suggests that the Si surface itself may be sterically or electronically inhibiting the reaction.

The XP spectra of the azide region of the azide-terminated surfaces itself has some interesting features. For instance, an experiment performed by a colleague showed that a third peak at ~ 398 eV appears in the nitrogen region when HMPA is used as a

solvent and as a function of reaction time (Figure 5.14). This peak is not present when MeOH is used as the solvent. Also, Si oxidation is observed in the glovebox after long reaction times with HMPA. This third peak, however, is not directly correlated with surface oxidation. The peak at 398 eV does not change after
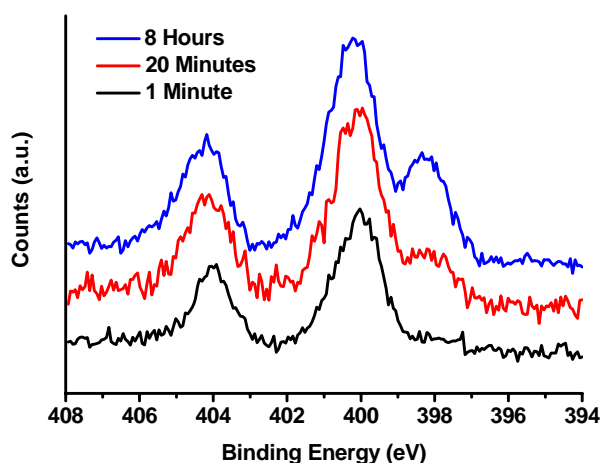
Figure 5.14. XP spectra of azide-terminated Si(111) surfaces after 1 minute (black), 20 minutes (red), and 8 hours (blue) reaction time using HMPA as the solvent

the substrate is explored to ambient conditions for several hours but the SiO_x peak continues to increase. Additionally, a third peak has been observed at ~ 407 eV when MeOH is used as solvent, which suggests the mechanism of azide-termination varies depending on the solvent choice. Further exploration of the mechanism behind the reaction and how it is affected by the solvent choice, and why the CuAAC reaction does not proceed readily on these surfaces is needed and will most likely reveal many interesting insights.

5.9   Conclusion

A new microcontact printing technique was developed that utilized a heterogeneous catalyst coated directly on the stamp. The Cu-catalyzed azide-alkyne cycloaddition was used to covalently attach interesting molecules onto Au or Si substrates. The heterogeneous catalyst reaction was shown to proceed almost as quickly as the homogeneous catalyst reaction. The benefits to using a heterogeneous catalyst is that the surfaces are not contaminated by residual catalyst and the Cu^{I} solubility issues in the ink are eliminated. Not only is 100% conversion achievable after ~ 1 hour of stamp time using a flat stamp, but patterns using patterned stamps are transferred to the substrates with high fidelity. It is expected that this technology will be important in making new molecular electronics devices and circuits easily and quickly.

5.10   References

1.   Xia, Y.; Whitesides, G. M. Soft Lithography. *Angew. Chem. Int. Ed.* **1998,** 37, 550–575.

2.   Kumar, A.; Whitesides, G. M. Features of Gold Having Micrometer to Centimeter Dimensions Can Be Formed Through a Combination of Stamping with an Elastomeric Stamp and an Alkanethiol "Ink" Followed by Chemical Etching. *Appl. Phys. Lett.* **1993,** 63, 2002–2004.

3.   Goetting, L. B.; Deng, T.; Whitesides, G. M. Microcontact Printing of Alkanephosphonic Acids on Aluminum: Pattern Transfer by Wet Chemical Etching. *Langmuir* **1999,** 15, 1182–1191.

4.   Jeon, N. L.; Finnie, K.; Branshaw, K.; Nuzzo, R. G. Structure and Stability of Patterned Self-Assembled Films of Octadecyltrichlorosilane Formed By Contact Printing. *Langmuir* **1997,** 13, 3382–3391.

5.   Rozkiewicz, D. I.; Janczewski, D.; Verboom, W.; Ravoo, B. J.; Reinhoudt, D. N. "Click" Chemistry by Microcontact Printing. *Angew. Chem. Int. Ed.* **2006,** 45, 5292–5296.

6.   Rozkiewicz, D. I.; Gierlich, J.; Burley, G. A.; Gutsmiedl, K.; Carell, T.; Ravoo, B. J.; Reinhoudt, D. N. Transfer Printing of DNA by "Click" Chemistry. *Chem. Bio. Chem.* **2007,** 8, 1997–2002.

7.   Rozkiewicz, D. I.; Ravoo, B. J.; Reinhoudt, D. N. Reversible Covalent Patterning and Self-Assembled Monolayers on Gold and Silicon Oxide Surfaces. *Langmuir* **2005,** 21, 6337–6343.

8.   Rozkiewicz, D. I.; Kraan, Y.; Werten, M. W. T.; Wolf, F. A. d.; Subramaniam, V.; Ravoo, B. J.; Reinhoudt, D. N. Covalent Microcontact Printing of Proteins for Cell Patterning. *Chem. Eur. J.* **2006,** 12, 6290–6297.

9.   Rozkiewicz, D. I.; Brugman, W.; Kerkhoven, R. M.; Ravoo, B. J.; Reinhoudt, D. N. Dendrimer-Mediated Transfer Printing of DNA and RNA Microarrays. *J. Am. Chem. Soc.* **2007,** 129, 11593–11599.

10.   Yan, L.; Zhao, X.-M.; Whitesides, G. M. Patterning a Preformed, Reactive SAM Using Microcontact Printing. *J. Am. Chem. Soc.* **1998,** 120, 6179–6180.

11.   Sullivan, T. P.; Poll, M. L. v.; Dankers, P. Y. W.; Huck, W. T. S. Forced Peptide Synthesis in Nanoscale Confinement under Elastomeric Stamps. *Angew. Chem. Int. Ed.* **2004,** 43, 4190–4193.

12. Lahiri, J.; Ostuni, E.; Whitesides, G. M. Patterning Ligands on Reactive SAMs by Microcontact Printing. *Langmuir* **1999,** 15, 2055–2060.

13. Green, J. E.; Choi, J. W.; Boukai, A.; Bunimovich, Y.; Johnston-Halperin, E.; DeIonno, E.; Luo, Y.; Sheriff, B. A.; Xu, K.; Shin, Y. S.; Tseng, H. R.; Stoddart, J. F.; Heath, J. R. A 160-Kilobit Molecular Electronic Memory Patterned at 10(11) Bits per Square Centimetre. *Nature* **2007,** 445, 414–417.

14. Wang, D.; Sheriff, B. A.; Heath, J. R. Silicon p-FETs from Ultrahigh Density Nanowire Arrays. *Nano Lett.* **2006,** 6, 1096–1100.

15. Wang, D. W.; Sheriff, B. A.; Heath, J. R. Complementary Symmetry Silicon Nanowire Logic: Power-Efficient Inverters with Gain. *Small* **2006,** 2, 1153–1158.

16. Luo, Y.; Collier, C. P.; Jeppesen, J. O.; Nielson, K. A.; DeIonno, E.; Ho, G.; Perkins, J.; Tseng, H.-R.; Yamamoto, T.; Stoddart, J. F.; Heath, J. R. Two-Dimensional Molecular Electronic Circuits. *Chem. Phys. Chem.* **2002,** 3, 519–525.

17. Collier, C. P.; Jeppesen, J. O.; Luo, Y.; Perkins, J.; Wong, E. W.; Heath, J. R.; Stoddart, J. F. Molecular-Based Electronically Switchable Tunnel Junction Devices. *J. Am. Chem. Soc.* **2001,** 123, 12632–12641.

18. DeIonno, E.; Tseng, H. R.; Harvey, D.; Stoddart, J. F.; Heath, J. R. Infrared Spectroscopic Characterization of [2]Rotaxane Molecular Switch Tunnel Junction Devices. *J. Phys. Chem. B* **2006,** 110, 7609–7612.

19. Jung, G. Y.; Johnston-Halperin, E.; Wu, W.; Z., Y.; Wang, S. Y.; Li, Z.; Green, J. E.; Sheriff, B. A.; Boukai, A.; Bunimovich, Y.; Heath, J. R.; Williams, R. S. Nanowire Circuit Fabrication at 34 nm Pitch by Nanoimprint Lithography. *Nano Lett.* **2006,** 6, 351–354.

20. Love, J. C.; Estroff, L. A.; Kriebel, J. K.; Nuzzo, R. G.; Whitesides, G. M. Self-Assembed Monolayers of Thiolates on Metals as a Form of Nanotechnology. *Chem. Rev.* **2005,** 105, 1103–1169.

21. Huang, J.; Hemminger, J. C. Photooxidation of Thiols in Self-Assembled Monolayers on Gold. *J. Am. Chem. Soc.* **1993,** 115, 3342–3343.

22. Haber, J. A.; Lewis, N. S. Infrared and X-ray Photoelectron Spectroscopic Studies of the Reactions of Hydrogen-Terminated Crystalline Si(111) and Si(100) Surfaces with Br_2, I_2, and Ferrocenium in Alcohol Solvents. *J. Phys. Chem. B* **2002,** 106, 3639–3656.

23. Webb, L. J.; Lewis, N. S. Comparison of the Electrical Properties and Chemical Stability of Crystalline Silicon(111) Surfaces Alkylated Using Grignard Reagents or Olefins with Lewis Acid Catalysts. *J. Phys. Chem. B* **2003,** 107, 5404–5412.

24. Collman, J. P.; Devaraj, N. K.; Eberspacher, T. A.; Chidsey, C. E. D. Mixed Azide-Terminated Monolayers: A Platform for Modifying Electrode Surfaces. *Langmuir* **2006,** 22, 2457–2464.

25. Porter, M. D.; Bright, T. B.; Allara, D. L.; Chidsey, C. E. D. Spontaneously Organized Molecular Assemblies. 4. Structural Characterization of n-Alkyl Thiol Monolayers on Gold by Optical Ellipsometry, Infrared Spectroscopy, and Electrochemistry. *J. Am. Chem. Soc.* **1987,** 109, 3359–3368.

26. Chaundhry, M. T.; R., S. Aromatic Polyfluoro Compounds. XIV. Phenylation of Hexafluorobenzene and Some Replacement Reactions of 2,3,4,5,6-Pentafluorobiphenyl. *J. Chem. Soc.* **1963** (Aug.) 4281–4283.

27. Meyer, E.; Overney, R. M.; Dransfeld, K.; Gyalog, T. *Nanoscience: Friction and Rheology on the Nanometer Scale*. World Scientific Publishing Company: River Edge, NJ, **1999**.

28. Bard, A. J.; Faulkner, L. R. *Electrochemical Methods: Fundamentals and Applications*. (Second ed.) John Wiley and Sons, Inc.: Hoboken, NJ, **2001**.

29. Piston, D. W.; Kremers, G.-J. Fluorescent protein FRET: the good, the bad and the ugly. *Trends in Biochemical Sciences* **2007,** 32, 407–414.

30. Kolb, H. C.; Finn, M. G.; Sharpless, K. B. Click Chemistry: Diverse Chemical Function from a Few Good Reactions. *Angew. Chem. Int. Ed.* **2001,** 40, 2004–2021.

31. Rozkiewicz, D. I. Personal Communication. Pasadena, CA, **2007**.

32. Masel, R. I. *Principles of Adsorption and Reaction on Solid Surfaces*. John Wiley and Sons, Inc.: New York, **1996**.

33. McQuarrie, D. A.; Simon, J. D. *Physical Chemistry: A Molecular Approach.* University Science Books: Sausalito, CA, **1997**.

34. Rostovtsev, V. V.; Green, L. G.; Fokin, V. V.; Sharpless, K. B. A Stepwise Huisgen Cycloaddition Process: Copper(I)-Catalyzed Regioselective "Ligation" of Azides and Terminal Alkynes. *Angew. Chem. Int. Ed.* **2002,** 41, 2596–2599.

35. Tornoe, C. W.; Christensen, C.; Meldal, M. Petidotriazoles on Solid Phase: [1,2,3]-Triazoles by Regiospecific Copper(I)-Catalyzed 1,3-Dipolar Cycloadditions of Terminal Alkynes to Azides. *J. Org. Chem.* **2002,** 67, 3057–3064.

36. Bock, V. D.; Hiemstra, H.; Maarseveen, J. H. v. Cu(I)-Catalyzed Alkyne-Azide "Click" Cycloadditions from a Mechanistic and Synthetic Perspective. *Eur. J. Org. Chem.* **2006**, 51–68.

37. Lipshutz, B. H.; Taft, B. R. Heterogeneous Copper-in-Charcoal-Catalyzed Click Chemistry. *Angew. Chem. Int. Ed.* **2006,** 45, 8235–8238.

38. Pachon, L. D.; Maarseveen, J. H. v.; Rothenberg, G. Click Chemistry: Copper Clusters Catalyse the Cycloaddition of Azides with Terminal Alkynes. *Adv. Synth. Catal.* **2005,** 347, 811-815.

39. Thathagar, M. B.; Beckers, J.; Rothenberg, G. Palladium-Free and Ligand-Free Sonogashira Cross-Coupling. *Green Chem.* **2004,** 6, 215–218.

40. Tsoncheva, T.; Vankova, S.; Mehandjiev, D. Effect of the Precursor and the Preparation Method on Copper Based Activated Carbon Catalysts for Methanol Decomposition to Hydrogen and Carbon Monoxide. *Fuel* **2002,** 82, 755–763.

41. Iijima, J.; Lim, J.-W.; Hong, S.-H.; Suzuki, S.; Mimura, K.; Isshiki, M. Native Oxidation of Ultra High Purity Cu Bulk and Thin Films. *Appl. Surf. Sci.* **2006,** 253, 2825–2829.

42. Linford, M. R.; Chidsey, C. E. D. Alkyl Monolayers Covalently Bonded to Silicon Surfaces. *J. Am. Chem. Soc.* **1993,** 115, 12631–12632.

43. Linford, M. R.; Fenter, P.; Eisenberger, P. M.; Chidsey, C. E. D. Alkyl Monolayers on Silicon Prepared from 1-Alkenes and Hydrogen-Terminated Silicon. *J. Am. Chem. Soc.* **1995,** 117, 3145–3155.

44. Buriak, J. M. Organometallic Chemistry on Silicon and Germanium Surfaces. *Chem. Rev.* **2002,** 102, 1271–1308.

45. Rohde, R. D.; Agnew, H. D.; Yeo, W.-S.; Bailey, R. C.; Heath, J. R. A Non-oxidative Approach toward Chemically and Electrochemically Functionalizing Si(111). *J. Am. Chem. Soc.* **2006,** 128, 9518–9525.

46. Baskin, J. M.; Prescher, J. A.; Laughlin, S. T.; Agard, N. J.; Chang, P. V.; Miller, I. A.; Lo, A.; Codelli, J. A.; Bertozzi, C. R. Copper-Free Click Chemistry for Dynamic In Vivo Imaging. *Proc. Natl. Acad. Sci. U.S.A.* **2007,** 104, 16793–16797.